UNIVERSITY OF OKLAHOMA

GRADUATE COLLEGE

AUTOMATED ALGORITHM FOR OPTICAL COHERENCE TOMOGRAPHY (OCT) IMAGES OF 3D SPHEROIDS

A THESIS

SUBMITTED TO THE GRADUATE FACULTY

in partial fulfillment of the requirements for the

Degree of

MASTER OF SCIENCE

By

TRISHA VALERIO

Norman, Oklahoma

2020

AUTOMATED ALGORITHM FOR OPTICAL COHERENCE TOMOGRAPHY (OCT) IMAGES OF 3D SPHEROIDS

A THESIS APPROVED FOR THE

STEPHENSON SCHOOL OF BIOMEDICAL ENGINEERING

BY THE COMMITTEE CONSISTING OF

Dr. Qinggong Tang, Chair

Dr. Handan Acar

Dr. Han Yuan

Table of Contents

Abstract

The application of three-dimensional (3D) tumor spheroids has been expanding due to their ability to closely mimic several features of solid tumors such as their cellular heterogeneity/organization and growth kinetics. Optical Coherence Tomography (OCT) system has been utilized to characterize 3D morphological and physiological information of multicellular tumor spheroids. In order to characterize and analyze the results of 3D OCT spheroid datasets, there is a need to develop an automated algorithm with high accuracy that can calculate the volume of a tumor spheroid and its necrotic tissues. The developed automated algorithm can automatically detect the margin of the 3D tumor spheroids and its necrotic region. The measurements from the automated program were then compared with the manual method to assess the accuracy of the developed algorithm through calculations of the Dice coefficient, and the results show a Dice number of 0.9449 and 0.9145 for spheroid and necrotic volume algorithms, respectively. Additionally, curve fitting was performed to further study the growth kinetics of the spheroid and its necrotic tissues, and measures such as root-mean-square error (RMSE) and corrected Akaike information criterion (AICc) were taken for this assessment. According to the RMSE measure, Boltzmann was the best fitted model for the overall spheroid volume growth. Logistic model, on the other hand, was best fitted in modeling the growth of necrotic core according to both RMSE and AICc values. Quantification of the spheroid volume (and its necrotic core) is significant as morphological features are often related to tumor activities, and determination of the best model is also vital in predicting the behavior of the spheroids. Overall, the algorithm used for this study allows for more efficient, in both time and accuracy, studies such as evaluating the growth medium's effect on tumor spheroids, growth characterization of varying cell lines, as well as the efficacy of a certain drug.

1 Introduction

Cancer occurs when the ordered process of cell division fails, and this results in an uncontrolled and abnormal growth of tissues called tumor. This disease has greatly impacted our society as its mortality remains high despite all developments in medicine and research. According to the National Cancer Institute's (NCI) estimation, around 1.8 million people in the United States[1], alone, will be diagnosed with cancer in 2020, and this disease is still the second leading cause of death, worldwide.[2] In fact, the NCI also approximated that roughly 600,000 deaths due to cancer will occur in 2020 in the United States[1]. Treatments of this disease include surgery, chemotherapy, targeted therapy, and immunotherapy, and due to the success and evolution of these therapies, the global mortality rate of cancer has decreased, especially in the last twenty years.[3]

In order to improve these methods of treatment, it is highly critical to understand how cancer cells and tumors behave, and many research studies are currently being conducted in order to explore tumor's properties, characteristics, and interactions with other cells and tissues. The development of new anticancer drugs often fails (90%- solid tumors) due to lack of efficacy or presence of toxicity during clinical trials, and researchers have suggested that utilization of oversimplistic cell cultures during *in vitro* testing may be the cause of this problem.[4] *In vitro* modeling is the first phase of new drug development and it is especially critical as results from this step greatly influence the rest of the phases. Two-dimensional (2D) cell cultures are often used in this phase due to its advantages—cultured within minutes to hours, cheap and reproducible, and its simplicity allows for an easy interpretation of data.[5] These models are extremely useful, but the development of 3D cultures has evolved drug discovery. Despite its disadvantages (longer culture formation time, worse reproducibility than 2D cultures, and cost), 3D cultures' potential in accurately modeling real tumors has been growing interest in the field of biotechnology. Tumor spheroids are one type of the 3D models, and these are 3D cellular aggregates (micron-sized) used to model different cancer types. They can better mimic real tumors as cell-cell/cell-extracellular matrix interactions exist, cellular organization (from necrotic to proliferation layers) is also present, and growth kinetics are similar to that of solid tumors.[6] Structural changes and potential drug resistance (due to 3D organization) of these spheroids further enhances its functionality and effectiveness over 2D cultures.

Another major advantage of 3D spheroid is the presence of three zones that make up the spheroid—proliferative, quiescent, and necrotic zones—but these sections are more apparent in larger spheroids. The proliferative zone is the outermost layer of the spheroid, and this region is the only part in which cells proliferate as it receives enough supply of nutrients and oxygen to grow.[7] The second region, quiescent, can be found between the proliferative and necrotic zones, and its cells are still alive but no longer proliferating. Finally, necrotic zone is the innermost layer [core] of the tumor spheroid, and this region is especially evident in older cultures as [quiescent] cells die due to lack of oxygen and nutrients.[8] Quantification of these biological zones in the tumor spheroid is significant as scientists can better optimize dose prescription and drug-response prediction. This study will, therefore, characterize and analyze the growth volume of one of these zones, necrotic region, using the developed automated algorithm.

In terms of imaging, bright field microscopy, phase contrast imaging, and fluorescence microscopy are often used to image the tumor spheroids but only 2D images can be obtained from these modalities, hence, 3D structures of the spheroids cannot be observed. Loss of signal can also occur while imaging using these techniques as volumes and depths of the spheroids can sometimes be large and the penetration depth for these conventional microscopies are often limited to 50 microns. Light sheet microscopy (LSM) is another option to image these models, but preparation of samples usually involves numerous and time-consuming steps, thus, an imaging modality that can overcome these issues is needed.[9] Optical coherence tomography (OCT) is an imaging modality that applies the principles of low-coherence interferometry to obtain 3D images of the specimen. OCT is also a label-free optical imaging modality with micron-sized resolution and penetration depth of a few millimeters[10] (depth of penetration can be adjusted by using longer wavelengths) so this technique overcomes one of the major hurdles of bright-field, phase-contrast and fluorescence imaging—imaging depth.

1.1. Purpose of the Study

Spheroid datasets imaging by OCT often consist of hundreds to a thousand cross-sectional images, and there is a need to develop an algorithm to analyze these images time-efficiently while maintaining accuracy. Some researchers simply use the diameter of the spheroid for their volume calculations, and this method assumes that the spheroid is a perfect sphere but this is not the case so this method can result in errors in their calculations. Other researchers also use well-known image analysis software, and while these are great and may result in accurate calculation, it may be time-consuming to adjust several parameters between batches of images. The objective of this study, therefore, was to develop an algorithm to measure the spheroids' volumes in a short period of time while maintaining a high accuracy. This study employed a swept-source OCT system to visualize the 3D volume of ovarian cancer cell line (OVCAR-8) spheroids with two different cell seeding density (5,000 cells/well and 50,000 cells/well) while implementing image processing algorithm to quantify the volume growth over a period of 18 days (5,000 cells/well will be referred to as the 5,000 group while 50,000 cells/well will be the 50,000 group for the remainder of the paper). Additionally, this study tested different mathematical models to determine the best fitted curve for the spheroid's volumetric growth and demonstrated OCT's ability to characterize necrotic core volume within the spheroids. The developed algorithm is significant as it allows for more efficient studies such as evaluating the growth medium's effect on tumor spheroids, growth characterization of various cell lines, as well as the efficacy of a certain drug. The curve fitting of mathematical models against the data points can also be crucial in drug-response prediction and dose prescription studies.

2 Methodology

2.1. OCT System

To determine the 3D volume of the spheroids, a swept-source OCT (SS-OCT) system was employed to acquire numerous 2D cross sectional images of the spheroids. The SS-OCT has an

imaging depth of 8.0 mm and 6.0 mm for air and water, respectively. The system also has a theoretical lateral resolution of 20 µm and axial resolution of 14 µm/10.6 µm for air/water. Additionally, the A-scan/Line rate for the system is 200 kHz with a sensitivity of 98 decibels. The schematic for the OCT system is shown in Figure 1 where the light source splits into two (through an optical coupler, OC)—one for the reference arm and another for the sample arm. The light in the sample arm images the spheroids in the well plate and light (from reference and sample) is then reflected back to the data acquisition board and computer for the recombination of reflected light and interference to eventually yield 2D images of the sample.

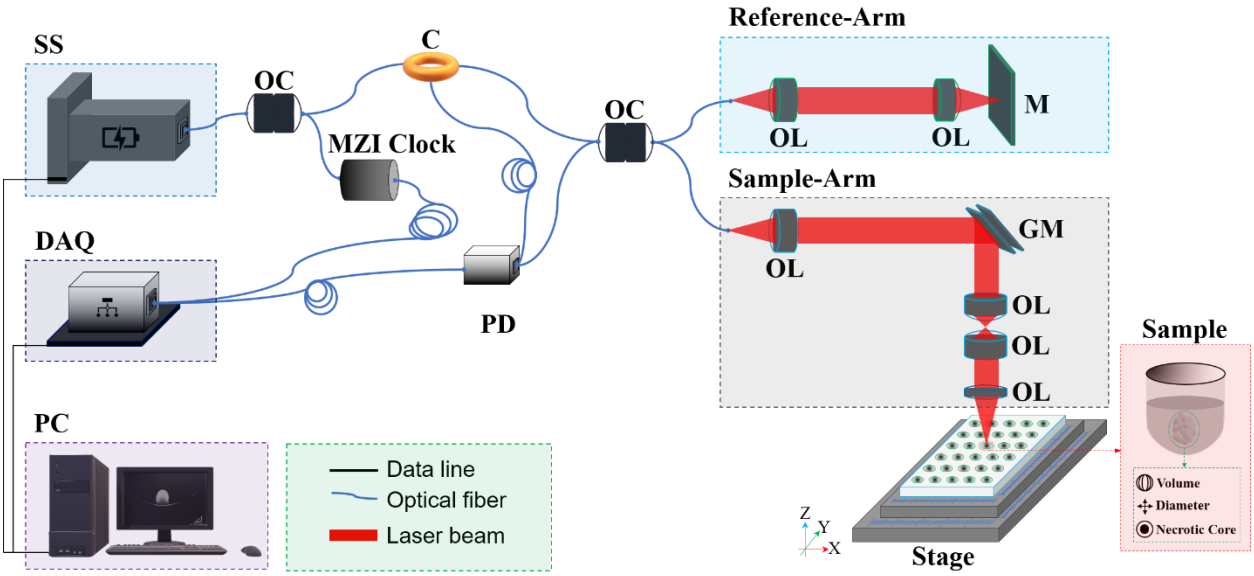

Fig. 1. Schematic of a SS-OCT system for 3D imaging of tumor spheroids. SS, swept-source. DAQ, data acquisition board. PC, computer. OC, optical coupler. MZI, Mach-Zehnder interferometer. C, circulator. PD, photodetector. OL, optical lens. M, mirror. GM, Galvanometer scanning mirror.

2.2. Image Acquisition and Processing

All tumor spheroid (OVCAR-8) samples were fixed then imaged using the OCT system. There were a total of two groups (based on cell seeding density) of spheroids used in this study: 5,000 [cells/well] (low cell seeding density) and 50,000 [cells/well] (high cell seeding density) group. For each group, there were 5 samples (spheroids) per day with the exception of day 11 to 18 of 50,000 group which only had 3 samples per day.

Cross-sectional images from the OCT software (ThorImageOCT) were exported for volume calculation, and these group of images were filtered so that only slices with signals from spheroids were acquired. The images were initially cropped to obtain the region-of-interest (ROI), and mid-section slice of the spheroid was cropped first followed by the rest of the slices. It was critical that the dimensions of the mid-section slice were obtained in the first place since these dimensions contain all signals of the spheroid for all slices. Some cropped 2D images had some level of noise

in the background so a denoising step was performed for all images using a gaussian filter. Detection of the boundary of the spheroid was then conducted, and this was accomplished by detecting the edges of the image using the Sobel operator and dilating the pixels with a spherical structuring element. Through this dilation step, the pixels were connected, and since some parts within the spheroids had no signal, filling the holes within the ROI was done to avoid inaccurate volume calculations. Finally, smoothing the edges (erosion) of the image was also executed using the same structuring element as the dilation step (spherical structuring element: size=3). The pixels within the boundary were then added up for an area calculation, and summation of area from all slices resulted in the spheroid's volume. MATLAB was used to perform the algorithms. The schematic of this process is shown in Figure 2.

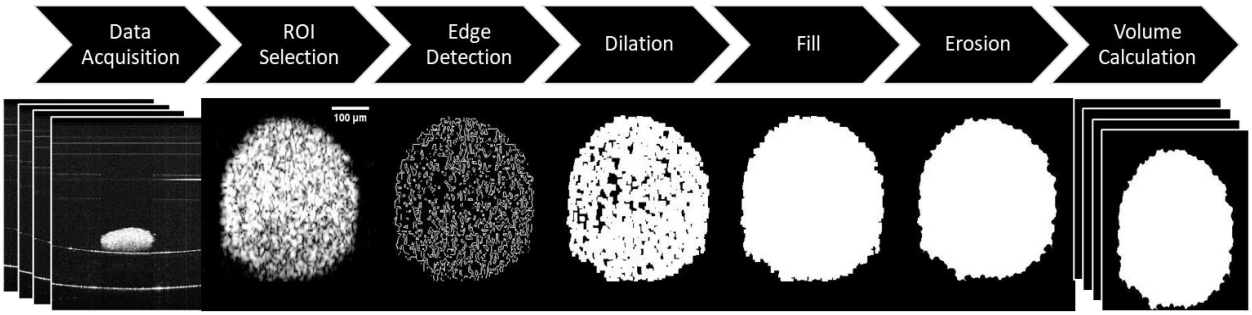

Fig. 2. Schematic diagram of image processing sequence: Data acquisition, ROI selection, edge detection, dilation, fill, erosion, area calculation, and volume calculation. *ROI Selection*, interactive cropping tool. *Edge Detection*, threshold: 0.07. *Dilation*, sphere-shaped structuring element: radius-3, lines. *Fill*, 'holes'. *Erosion*, sphere-shaped structuring element: radius-3.

2.3. 3D Spheroid Volume Calculation

In order to calculate the total volume for each spheroid, the number of pixels in a slice were initially added together, and this resulting value represents the area of the cross-sectional image. Areas from all cross-sectional images were then combined to quantify the total volume of the spheroid. This volume calculation was done for each spheroid over the duration of the experiment, 18 days, and since the volume is in pixels, this number was converted to cubic microns, μm^3 (by multiplying pixel values with the dimensions of the voxel).

2.4. Mathematical Modeling of the Spheroid Growth Curve

Four modeling curves were fitted to the volumetric growth data of tumor spheroids to further describe tumor's growth in volume, mathematically. These growth curves include logistics and Gompertz models (previously observed to potentially model the growth of tumor spheroids),[9] Boltzmann sigmoidal (used to model avascular tumor growth),[11] and exponential-linear model (one of the common macroscopic growth models).[12] The exponential-linear model is considered to be one of the simplest models in modeling tumor growth, and this function can be described by

an initial exponential growth followed by a linear phase. Logistics and Gompertz models, on the other hand, are known to model organ and organism's growth, and these models usually have sigmoidal shape—a curve with one inflection point which eventually converges to the sample's maximum volume.[13] Lastly, the Boltzmann curve is mostly used in fluid flow measurements and modeling, but several studies also associated this model with avascular tumor growth, and this curve also possess a sigmoidal shape. These four models have been previously studied but not compared relative to one another, and this is one innovation of this study. The best fitted model was determined by analyzing goodness-of-fit measures between each nonlinear model: root-mean-square error (RMSE) and Akaike information criterion with correction for small sizes (AICc) using GraphPad Prism. Additional residual plots were also provided, and paired t-tests were performed (using GraphPad Prism, as well) to determine if there were significant differences between each model. Finally, a p-value of <0.05 was used to indicate significant differences between each measurement.

2.5. Necrotic Core Identification

In its entirety, a spheroid is a 3-layer volume with the outermost layer being the proliferative zone, the middle layer constituting the quiescent zone, and the innermost layer making up the necrotic region. This necrotic tissue was identified in this study through calculation of tissue extinction coefficients (or slope of axial attenuation). Signals from the OCT represents detected back-scattering of light at various depths, so the OCT intensity function can then be described with the Beer-Lambert Law.[14] The extinction coefficient, μ, can be estimated by fitting the OCT intensity profiles with the Beer-Lambert model:

$$I(z) = I_0 e^{-2\mu z}$$

where μ represents the tissue extinction coefficient and z represents depth. Light attenuation in the necrotic regions may be due to the increase in the tissue extinction coefficient, thus, this value, μ, will be used to identify the margin of the necrotic tissue within the spheroids.[14]

ROI Selection, filtering methods, and morphological operation sequences were also used to identify the necrotic region of each slice. The images were initially cropped to obtain the ROI, and median filtering with a 10-by-10 neighborhood size was also applied to all images. Tissue extinction coefficients were then calculated, and thresholding was performed to specifically identify the necrotic core—the threshold values were determined by the histology images of the spheroids. After thresholding, morphological operations were, again, performed to filter images to match necrotic core region in the histology.

2.6. Volume Calculation and Mathematical Modeling of the Necrotic Region Growth Curve

After the detection and identification of the necrotic region of the spheroids, volume calculations were performed. Similar to the 3D spheroid volume calculation, areas values for each 2D cross-

sectional slice were summed up, and this results in a calculated volume for the spheroid. After plotting the volumetric data for both 5,000 and 50,000 groups, curve fitting using two basic models were executed: exponential-linear and logistic models. RMSE and AICc measures were also taken in order to evaluate the growth kinetics of the necrotic core, quantitatively.

3 Results

3.1 Accuracy of Automated Algorithm

Manually traced images of the spheroid were taken [as gold standards] to determine the accuracy of the segmented images. Three volunteers manually traced the outline of the spheroid for three different images (9 total images), and these images were used as ground truth images in Dice coefficient calculations. The Sørensen–Dice coefficient is mostly used in image segmentation, and this value represents the similarity between ground truth and segmented images. This value ranges from 0 to 1 with 0 meaning no overlap (between ground truth and segmented image) and 1 representing a total or perfect overlap between ground truth and segmented images—higher Dice score indicates higher similarity and accuracy between two images. The manual tracing of spheroid for accuracy assessment is shown in Figure 3.

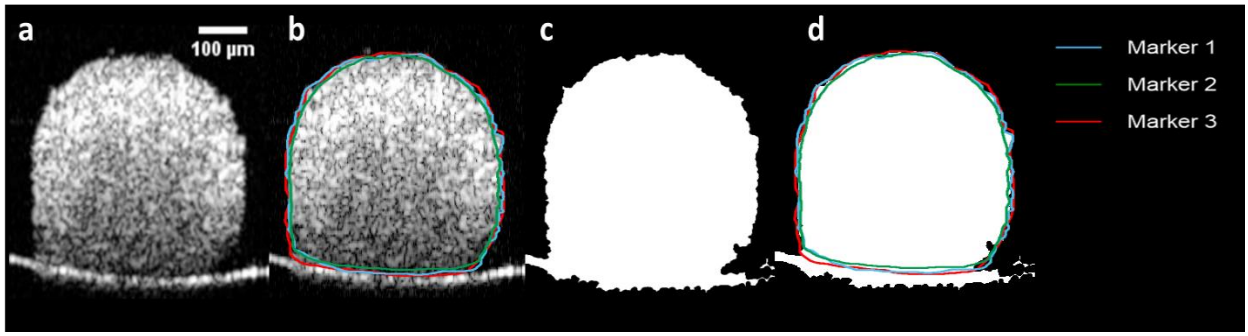

Fig. 3. Manual tracing of spheroid for accuracy assessment of algorithm through boundary tracing by 3 volunteers (markers). a) OCT image, b) manual profiles (outlines) on OCT image, c) processed image, d) manual profiles on processed image

The image processing algorithm presented above was selected by finding the best combination of edge detection threshold and morphological operations. The following values for sensitivity (edge detection threshold) were tested: 0.04, 0.05, 0.06, 0.07, 0.08, and 0.09. With regards to morphological operations application, methods with only dilation and methods with a combination of dilation and erosion were tested. For these operations, two structuring elements were used: disk structuring element (radius=3) and spherical structuring element (size=3). Table 1 shows the Dice coefficients after using a specific combination of edge detection threshold and morphological operation sequence. Application of 0.07 edge detection sensitivity while dilating and eroding the images with spherical structuring element resulted in the best Dice coefficient, 0.9449. This

coefficient represents the similarity between the ground truth image (manually traced) and the processed image after implementation of the algorithm.

Table 1. Dice coefficients after combination of edge detection threshold and morphological operations sequence. Method sequence was dilation followed by erosion. If only one morphological operation is listed, no erosion was applied. S, spherical structuring element (size:3). D, disk-shaped structuring element (radius:3).

		Edge Detection Threshold					
		0.04	**0.05**	**0.06**	**0.07**	**0.08**	**0.09**
Dilation-Erosion	**S**	0.9118	0.9293	0.9340	0.9359	0.9375	0.9354
	D	0.9174	0.9326	0.9365	0.9381	0.9386	0.9174
	S-D	0.9393	0.9435	0.9445	0.9447	0.9432	0.9352
	D-S	0.9433	0.9447	0.9448	0.9443	0.9400	0.8873
	D-D	0.9402	0.9436	0.9444	0.9442	0.9408	0.8931
	S-S	0.9408	0.9441	0.9448	0.9449	0.9429	0.9342

3.2 Volumetric Growth of 3D Tumor Spheroids

The OCT system was used to take volumetric imaging of OVCAR-8 spheroids for both 5,000 and 50,000 groups each day for a total of 18 days. Figure 4 quantitatively shows the changes in volume of 5,000 (blue) and 50,000 (orange) groups. It was found that the initial averaged volume for the 5,000 group was $6.82X10^7 \pm 1.43X10^6$ μm^3 while 50,000 group's was $2.9X10^8 \pm 2.66X10^7$ μm^3. For both groups, initial decrease (from day 1 to 2) can be observed, and this volumetric decline shows that cells are still fusing and aggregating to form a solid spheroid.[12] After this slight decrease, volumes (for both groups) began to rapidly increase (5,000: day 2-7. 50,000: day 3-12), and this was followed by slight changes in volume for the 5,000 group and a plateau phase for the 50,000 group. The averaged final volume for the low cell seeding group (5,000) was $3.69X10^8 \pm 2.08X10^7$ μm^3 and high cell seeding group's (50,000) was $4.89X10^8 \pm 9.12X10^6$ μm^3.The average volumes for all time points for both groups are shown in Figure 4.

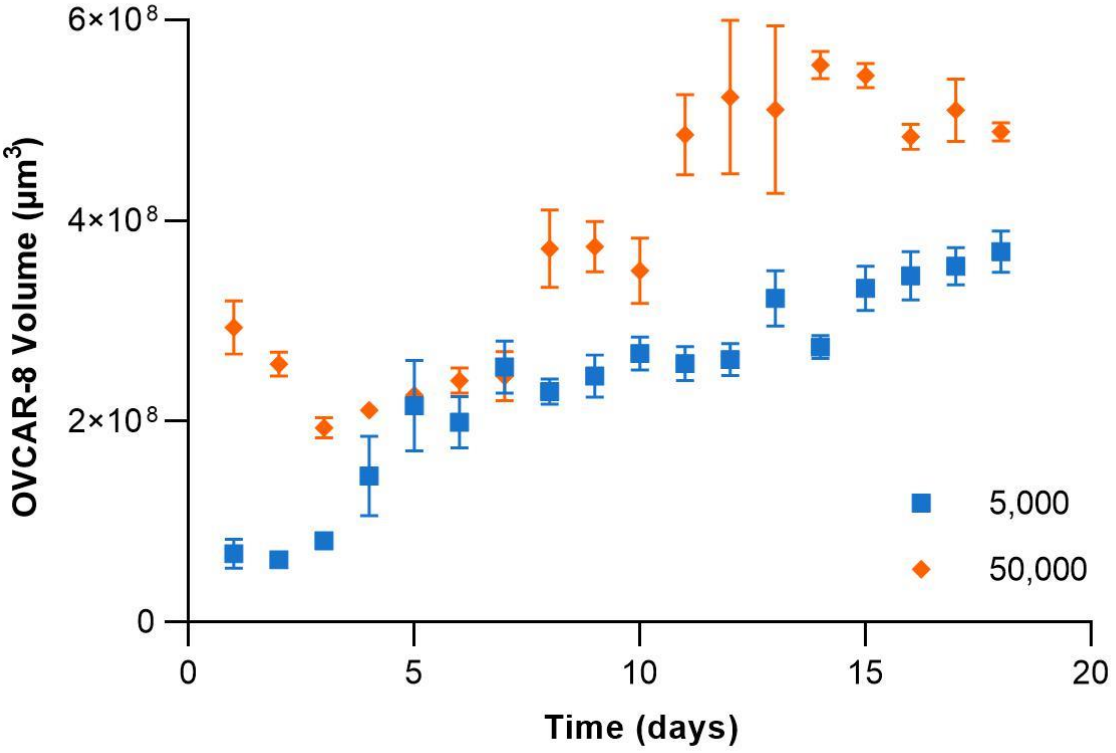

Fig. 4. OVCAR-8 volumes for both groups—5,000 cell seeding density [blue] and 50,000 cell seeding density [orange]. Data points are means ± standard deviations.

3.3 Mathematical Modeling

To further study the growth kinetics of the spheroid, quantitatively, modeling curves were fitted against the data points (both 5,000 and 50,000 groups) in Figure 5 with the four models mentioned earlier—exponential-linear (orange), Boltzmann sigmoidal (blue), logistic (green), and Gompertz (red). These models (especially exponential-linear, Gompertz and logistic) have been previously known as volumetric growth models of spheroids and tumors (using data from conventional microscopy), but no study has compared all four models together while using OCT, hence this study evaluated these models relative to one another to determine the best fit curve for spheroid growth.[9,10,11] Assessment of the best fitted curve can be useful in growth prediction, dose prescription, and drug-response prediction studies.

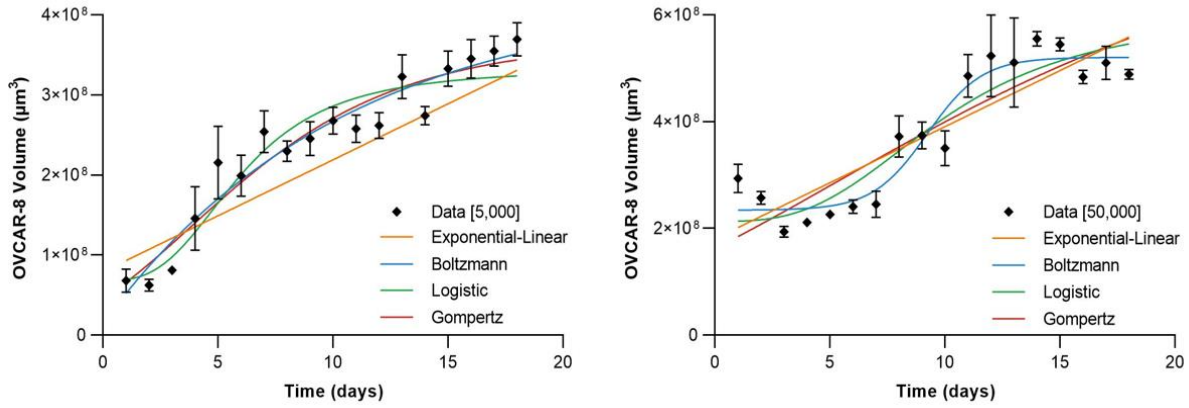

Fig. 5. Curve fitting with four models: exponential linear [orange], Boltzmann [blue], logistic [green], and Gompertz [red]. Fitted models are shown against 5,000 data [left] and 50,000 data [right]. Data points are means ± standard deviations.

3.4 Goodness-of-Fit

To assess the best model for the OVCAR-8 volumetric growth, two main approaches were taken: RMSE and AICc. RMSE is a statistical measure known to test how good the fit the model is to the data, and this is the square root of variance's residuals. RMSE values have the same units as the quantity being measure, and for this case, spheroid volume in µm^3. AICc, on the other hand, is a widely accepted measure to assess the quality between nonlinear models, and the equation for this measure is shown below:

$$AIC = 2K - 2\ln(L)$$

where K is the number of parameters and L is the log-likelihood estimate (the likelihood of model to yield the observed values). This measure is, therefore, unitless.

For both measures, lower values represent better fit of model to the dataset. It is important to analyze the AICc values relative to each other as AICc value, by itself, is not meaningful. RMSE and AICc average values for both cell seeding density groups are shown in Figure 6. The results of the RMSE assessment shows that the Boltzmann had the lowest RMSE for both 5,000 (RMSE = 2.44X10^7 µm^3) and 50,000 (RMSE = 3.64X10^7 µm^3) groups while exponential-linear model had the highest RMSE values (4.40X10^7 µm^3 and 6.16X10^7 µm^3 for 5,000 and 50,000 groups, respectively). In the AICc graph, on the other hand, AICc values of 5,000 group for Boltzmann, logistic, and Gompertz were almost similar to one another with values of 626.3, 629.0, and 624.8, respectively while exponential-linear's value was the largest at 652.2. The AICc values for the 50,000 groups were similar in trend as 50,000 RMSE values with increasing values starting from Boltzmann to logistic, Gompertz, and exponential-linear models. The summary figures for both goodness-of-fit measures are shown below.

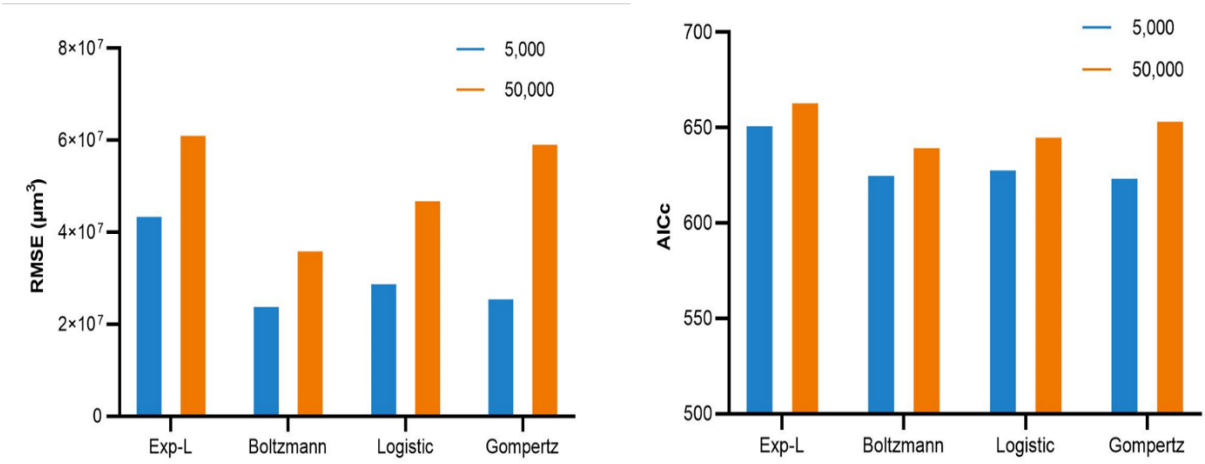

Fig. 6. RMSE [left] and AICc [right] values of all models (exponential-linear, Boltzmann, logistic, and Gompertz) for both 5,000 and 50,000 groups. Values of 5,000 group are shown in blue while 50,000's are shown in orange. RMSE, root-mean-square error. AICc, Akaike information criterion.

Additional residual graphs are also provided in Figure 7. Each plot represents each group (5,000 and 50,000), and the horizontal lines within the data set indicate the value of the mean for each model. Paired t-tests were also performed between each model, and only three pairs had statistically significant difference (all in the 5,000 group): exponential-linear/Boltzmann (p=0.0004), exponential-linear/logistic (p=0.0043), and exponential-linear/Gompertz (p=0.0003). The rest of the pairs in the 5,000 and 50,000 group had no significant differences. The residual plots for both groups are shown below.

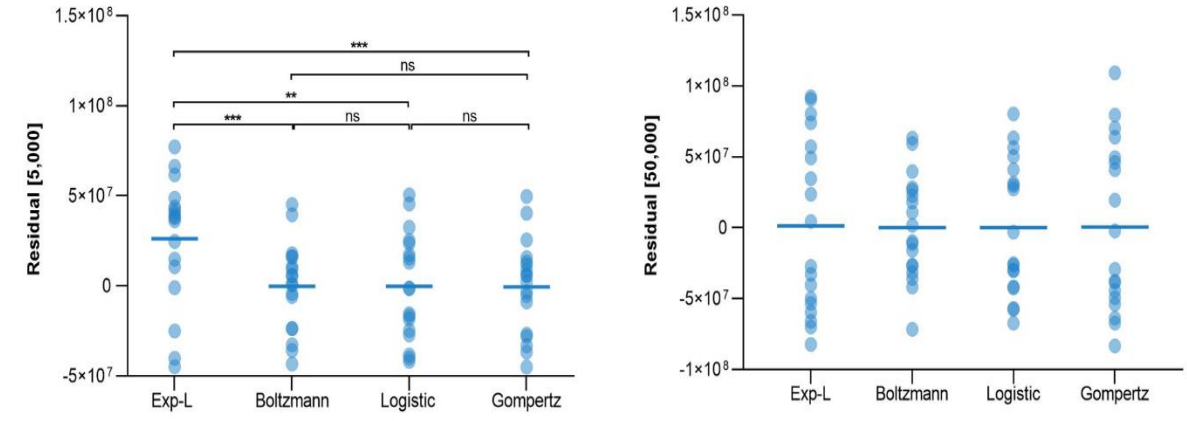

Fig. 7. Residual plots of the four models (exponential-linear, Boltzmann, logistic, and Gompertz). The plot for the 5,000 group is shown on the left while the plot for the 50,000 group is shown on the right. No significance between pairs were observed in the 50,000 group. ***: p-value<0.001. **: p-value<0.01.

3.5 Accuracy of Necrotic Region Algorithm

Accuracy measurement was also done—necrotic core region in the histology images were manually traced (3 total images for 3 different days), and these images were compared with processed images. Several thresholds (for attenuation coefficient) were tested in order to obtain the maximum Dice coefficient for the algorithm, and the results are shown in Figure 8. After applying these thresholds, the highest resulting Dice coefficient for the necrotic core identification algorithm was 0.9145 using the threshold value of 3.

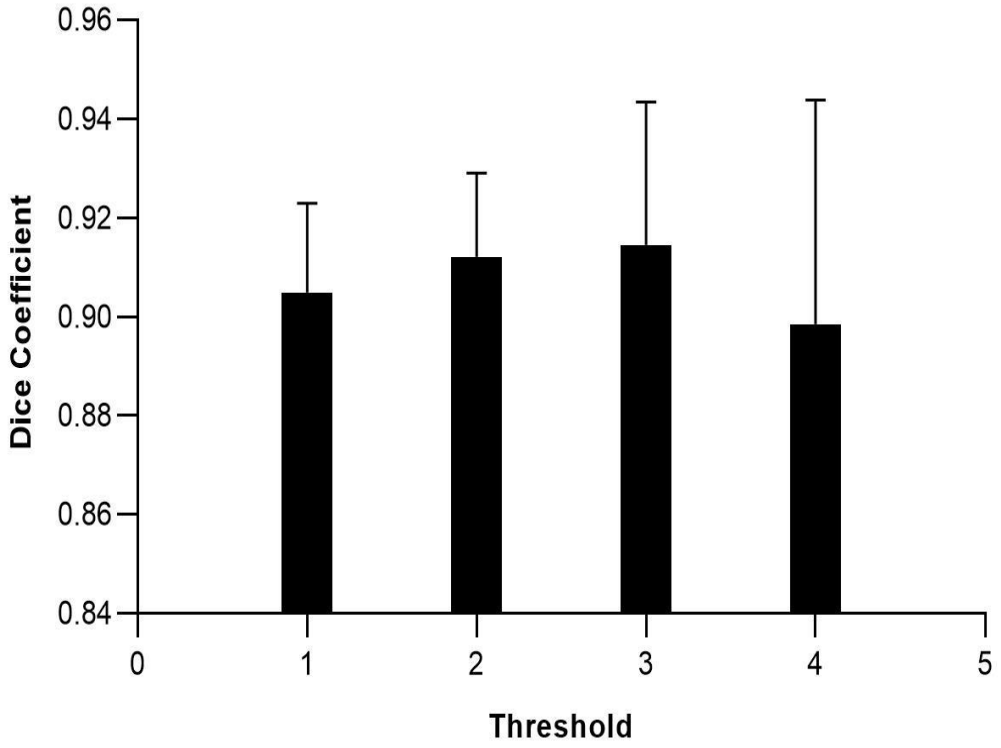

Figure 8. Dice coefficients after application of several threshold values (attenuation coefficient).

Additionally, the H&E-stained images, OCT images, processed images (after algorithm application) and OCT images overlay, and processed images and histology images overlay are shown in Figure 9. Necrotic core calculation was performed for both low and high cell seeding density groups.

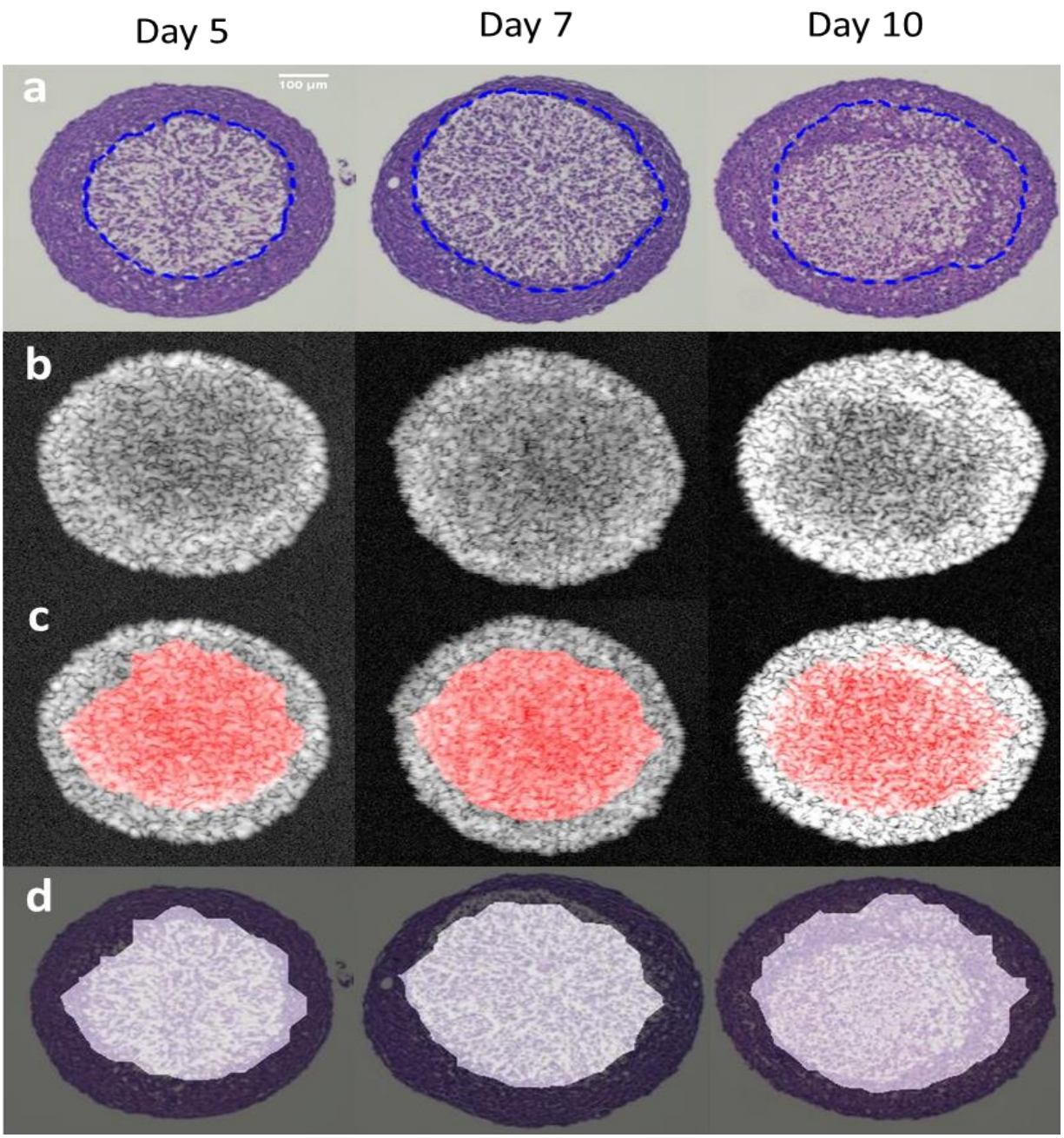

Fig. 9. Necrotic core detection accuracy using histology results from days 5, 7, and 10. a) histology images, b) original OCT images, c) processed images [red] (after algorithm application) and original OCT image overlay, d) histology [dark] and processed images [bright] overlay.

3.6 Volumetric Growth of Necrotic Core

After 2D cross-sectional images of the spheroids were taken, optical attenuation coefficient calculations followed by filtering methods (mentioned earlier) were performed to identify the necrotic region of the spheroid. Similar process as volume calculation for the entirety of the

spheroids was then executed—all pixels in each slice were added up for an area value then area for all cross-sectional images were summed up to quantify the volume. Necrotic core calculations were performed on both low (5,000) and high (50,000) cell seeding density groups. The volumetric growth of the necrotic core for both groups is shown in Figure 10 where each data point represents the averaged necrotic region volume for each time point for a total of 18 data points per group. This graph shows that in the early cultures (day1-3), necrotic tissues are almost non-existent in the spheroids then it consistently increased until day 10, and after day 10, a plateau phase can be seen. The final average necrotic core volume for the 5,000 group was $1.22X10^8 \pm 2.51X10^7$ μm^3 while the final volume (average) for the 50,000 group was $1.48X10^8 \pm 2.51X10^7$ μm^3. The overall volumetric growth of the necrotic tissues over 18 days is shown in Figure 10.

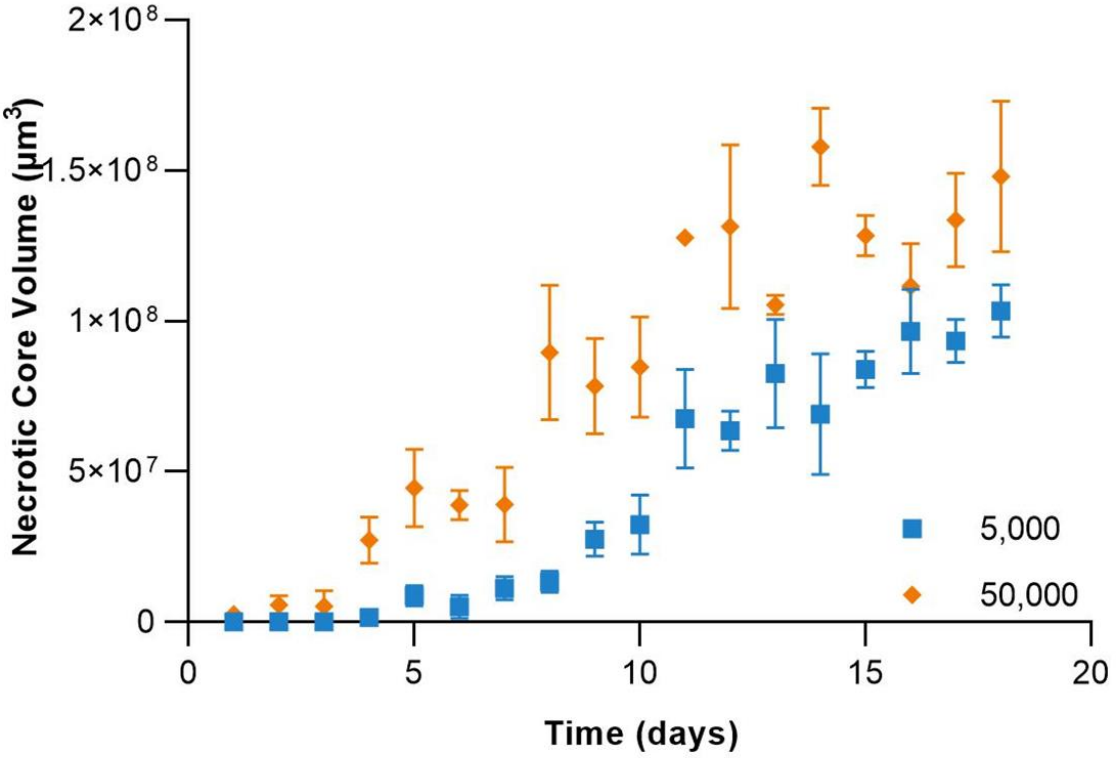

Fig. 10. Necrotic core volumes for the 5,000 [blue] and 50,000 [orange] groups. Data points are means ± standard deviations.

3.7 Mathematical Modeling for Necrotic Region Growth

Again, to study the growth kinetics of the necrotic region, quantitatively, curve fitting against the data points were performed for both groups. Two basic functions (exponential and sigmoidal) were used in this curve fitting section—the exponential-linear and logistic models. These modeling curves fitted against the data points are shown in Figure 11.

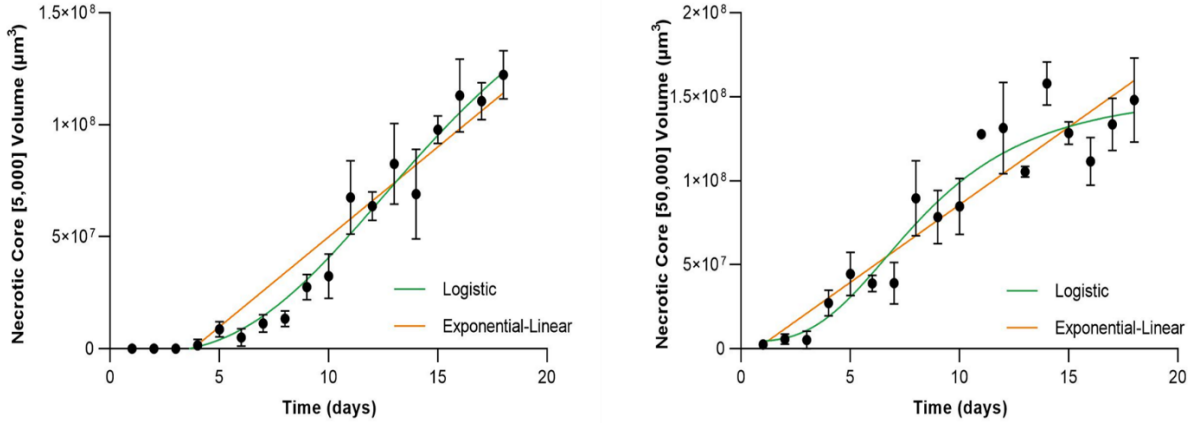

Figure 11. Curve fitting with two models: exponential linear [orange] and logistic [green]. Fitted models are shown against 5,000 data [left] and 50,000 data [right]. Data points are means ± standard deviations.

3.8 Goodness-of-Fit

Two main approaches were used to determine which of the two models best fit the necrotic core growth curve—RMSE and AICc measures. For both statistical measures, lower values indicate better fit, and for both the 5,000 and 50,000 groups, RMSE and AICc values were calculated and compared. The RMSE values for the logistic model were $7.21X10^6$ µm^3 and $1.48X10^7$ µm^3 for the 5,000 and 50,000 groups, respectively. These values are lower than the exponential-linear's RMSE values of $1.27X10^7$ µm^3 and $1.83X10^7$ µm^3 for the low and high cell seeding density groups, respectively. These results indicate that the logistic model is a better fit than the exponential-linear according to the RMSE measure. In terms of the AICc measure, the logistic model had AICc values of 578.5 and 604.5 for the 5,000 and 50,000 groups, respectively. The exponential-linear model, on the other hand, had values of 607.6 and 620.6, and these results indicate that the logistic model is, again, the better fit. The RMSE and AICc values are shown in Figure 12.

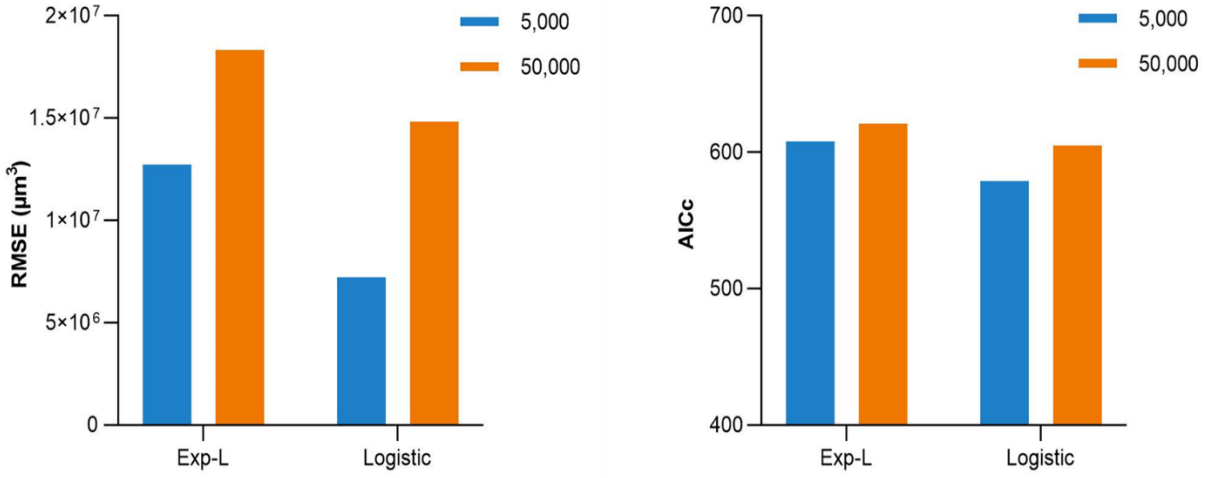

Fig. 12. RMSE [left] and AICc [right] of the exponential-linear and logistic models for both 5,000 and 50,000 groups. Values of 5,000 group are shown in blue while 50,000's are shown in orange. RMSE, root-mean-square error. AICc, Akaike information criterion.

Additional residual graphs are further provided in Figure 13. Each plot represents each group (low and high cell seeding density groups), and the horizontal lines mean values for each model. Paired t-tests were also performed between the two models, but no significant differences were observed for both the 5,000 and 50,000 groups. The residual plots for both groups are shown Figure 13.

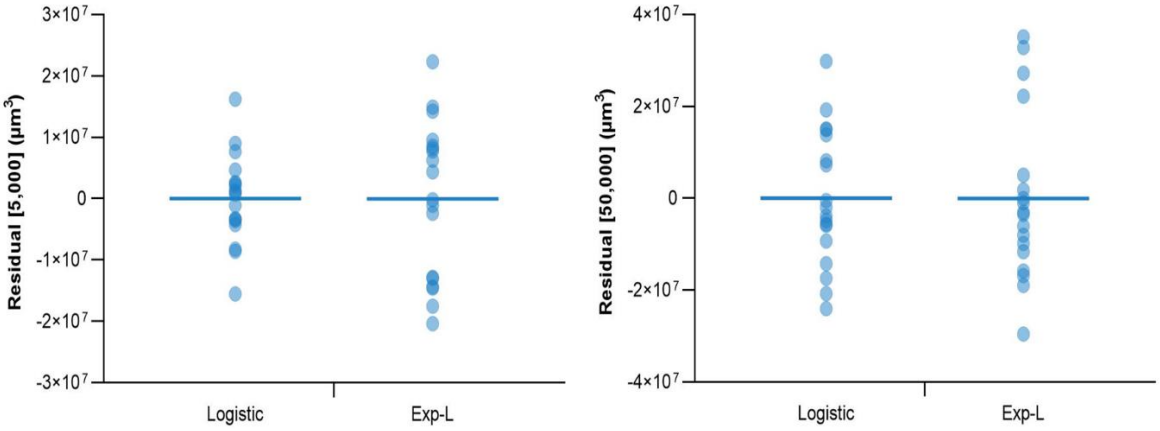

Fig. 13. Residual plots of the logistic and exponential linear models. The plot for the 5,000 group is shown on the left while the plot for the 50,000 group is shown on the right.

4 Discussion and Conclusion

Quantitative evaluation of 3D spheroids' growth curve and necrotic core volume is significant as morphological features of a tumor are often relevant in analyzing and predicting tumor activities.[14] Currently, 2D and 3D culture models are used in many oncological studies, but a tumor spheroid

(3D model) surpasses 2D models in this field of study in terms of mimicking real tumor behaviors. Many anti-cancer drugs fail, 90% failure in solid tumors, due to oversimplification in 2D *in vitro* models.[4] This study, therefore, utilized 3D spheroids. Tumor spheroids often consist of three layers—proliferative, quiescent, and necrotic—and the presence of these zones are critical in predicting the growth of tumors. Imaging of these models is another factor that is significant in evaluating the growth curves, accurately. Brightfield microscopy, phase-contrast microscopy, and even light sheet imaging have been well-established in viewing tumor spheroids but these modalities have disadvantages that prevent accurate calculation of volumes—loss of signal at greater depths and/or time-consuming sample preparation. These hurdles can be overcome by using OCT to image the 3D spheroids as OCT's penetration depth on biological tissue is around 1-3 mm compared to brightfield's several hundred microns penetration on tissue.[15] Additionally, OCT does not require any labels thus reducing the overall sample preparation time. This study, therefore, used OCT to image 3D spheroids along with an automated algorithm's application with the purpose of quantifying growth curve of the tumor volume and necrotic core volume.

An interesting observation in the growth curve of the spheroid for both groups is the initial decline from day 1 to day 2/3. This phenomenon was previously observed by other studies, and they claimed that during this phase, the cells are still aggregating and fusing to each other to form a solid spheroid.[16] The results of this experiment, thus, further solidifies that claim. The overall growth curve for both spheroids also seems to be similar to a sigmoidal shape, and this is consistent with previous studies in which they modeled the volumetric growth of spheroids.[9,11,17] Some studies also portrayed that spheroids, in early phases, grows quickly but once it reaches a maximum volume, this growth ceases, and this is again, consistent with the results of this experiment.[6] This, in a way, validates the accuracy of the OCT system and the developed algorithm. To assess this observation, various models were fitted against the data points for both groups, and according to the RMSE values, Boltzmann curve seems to fit best with the growth curve of OVCAR-8 (for both 5,000 and 50,000 groups). When assessed with AICc measure, however, it became difficult to differentiate the models from one another due to the proximity of the values relative to one another. Another measure was taken, residual plots, to determine whether there is any significant difference between each model. The results of this assessment show that in the 5,000 group, the exponential-linear model is significantly different from the other three models—it is the least fitted model against the growth data. For the residual plot of 50,000 group, on the other hand, no significance was observed in any of the pairs of models. It is, therefore, hard to conclude which of the four mathematical curves is best fitted for this study's data. More data samples may be necessary to find significant differences between each model. Additionally, necrotic tissue detection and calculations were also performed, and as mentioned earlier, necrotic volumes (especially for the 5,000 group) were almost non-existent earlier in the culture. This makes sense since necrotic core forms as a result of lack of nutrients and oxygen within the spheroid, and in earlier cultures, spheroids are still small, thus, all parts of the spheroid receive enough supply to live. Consistent volume growth was then observed for both groups, and this volume eventually reaches a plateau phase or minimal volume change as cultures age. Only two basic models were fitted (exponential-linear and logistic), and out of the two, the logistic model resulted in a better fit according to both the RMSE and AICc measures. In future studies, more spheroid samples and modeling curves can be applied in order to further enhance and solidify the results of this study.

In summary, this study's purpose was to develop an algorithm to calculate the volumes of the spheroid, and this is significant as morphology is often related to tumor activity and current volume calculation techniques can be time-consuming or inaccurate. The algorithm was developed using image segmentation and processing methods to accurately calculate the volumes of the spheroids, and the resulting Dice coefficients were 0.9449 (for spheroid volume calculation) and 0.9145 (for necrotic core volume calculation). Additionally, various mathematical models were fitted against the data points for both groups to further study the growth kinetics of the volumetric growths. In the spheroid volumetric curve, the Boltzmann sigmoidal model was the best fitted model according to the RMSE. In the necrotic core growth, on the other hand, the logistic model resulted in a better fit (according to both RMSE and AICc measures) compared to the exponential-linear model. The results show an efficient (in both time and accuracy) algorithm that was used to calculate the volumes of the spheroids and their necrotic cores. The calculation of necrotic core volumes (an innovation of this study) allows for more studies to be conducted (such as evaluating the effects of a drug in the necrotic volume of the spheroid), and overall, this study contributes and advances the knowledge of spheroid (and its necrotic core) growth so that in the future, better drugs can potentially be developed.

References

1. Surveillance, Epidemiology, and End Results (SEER) Program. Cancer Statistics. https://www.cancer.gov/about-cancer/understanding/statistics#:~:text=The%20rate%20of%20new%20cases,on%20201 3%E2%80%932017%20deaths). Accessed November 20, 2020.
2. Centers for Disease Control and Prevention. Leading Causes of Death. https://www.cdc.gov/nchs/fastats/leading-causes-of-death.htm. Accessed November 20, 2020.
3. Falzone L, Salomone S, Libra M. Evolution of Cancer Pharmacological Treatments at the Turn of the Third Millennium. *Front Pharmacol*. 2018;9:1300. Published 2018 Nov 13. doi:10.3389/fphar.2018.01300
4. Maeda H, Khatami M. Analyses of repeated failures in cancer therapy for solid tumors: poor tumor-selective drug delivery, low therapeutic efficacy, and unsustainable costs. *Clin Transl Med*. 2018;7(1):11. Published 2018 Mar 1. doi:10.1186/s40169-018-0185-6
5. Kapałczyńska M, Kolenda T, Przybyła W, et al. 2D and 3D cell cultures - a comparison of different types of cancer cell cultures. *Arch Med Sci*. 2018;14(4):910-919. doi:10.5114/aoms.2016.63743
6. Costa EC, Moreira AF, de Melo-Diogo D, Gaspar VM, Carvalho MP, Correia IJ. 3D tumor spheroids: an overview on the tools and techniques used for their analysis. *Biotechnol Adv*. 2016;34(8):1427-1441. doi: 10.1016/j.biotechadv.2016.11.002
7. Dini S, Binder BJ, Fischer SC, et al. Identifying the necrotic zone boundary in tumour spheroids with pair-correlation functions. *J R Soc Interface*. 2016;13(123):20160649. doi:10.1098/rsif.2016.0649
8. Wallace DI, Guo X. Properties of tumor spheroid growth exhibited by simple mathematical models. *Front Oncol*. 2013; 3:51. Published 2013 Mar 15. doi:10.3389/fonc.2013.00051
9. Sharma U, Chang EW, Yun SH. Long-wavelength optical coherence tomography at 1.7 micron for enhanced imaging depth. *Opt Express*. 2008;16(24):19712-19723. doi:10.1364/oe.16.019712
10. Huang Y, Wang S, Guo Q, et al. Optical Coherence Tomography Detects Necrotic Regions and Volumetrically Quantifies Multicellular Tumor Spheroids. *Cancer Res*. 2017;77(21):6011-6020. doi: 10.1158/0008-5472.CAN-17-0821
11. Ward JP, King JR. Mathematical modelling of avascular-tumour growth. *IMA J Math Appl Med Biol*. 1997;14(1):39-69.
12. West J, Newton PK. Cellular interactions constrain tumor growth. *Proc Natl Acad Sci U S A*. 2019;116(6):1918-1923. doi:10.1073/pnas.1804150116
13. Benzekry S, Lamont C, Beheshti A, et al. Classical mathematical models for description and prediction of experimental tumor growth. *PLoS Comput Biol*. 2014;10(8):e1003800. Published 2014 Aug 28. doi:10.1371/journal.pcbi.1003800
14. Tang Q, Wang J, Frank A, et al. Depth-resolved imaging of colon tumor using optical coherence tomography and fluorescence laminar optical tomography. *Biomed Opt Express*. 2016;7(12):5218-5232. Published 2016 Nov 21. doi:10.1364/BOE.7.005218

15. Kessel S, Cribbes S, Déry O, et al. High-Throughput 3D Tumor Spheroid Screening Method for Cancer Drug Discovery Using Celigo Image Cytometry. *SLAS Technol*. 2017;22(4):454-465. doi:10.1177/2211068216652846
16. Gong X, Lin C, Cheng J, et al. Generation of Multicellular Tumor Spheroids with Microwell-Based Agarose Scaffolds for Drug Testing. *PLoS One*. 2015;10(6):e0130348. Published 2015 Jun 19. doi: 10.1371/journal.pone.0130348
17. Grimes DR, Kannan P, McIntyre A, et al. The Role of Oxygen in Avascular Tumor Growth. *PLoS One*. 2016;11(4): e0153692. Published 2016 Apr 18. doi: 10.1371/journal.pone.0153692